Science and Technology Indonesia
e-ISSN:2580-4391 *p*-ISSN:2580-4405
Vol. 10, No. 2, April 2025

Research Paper

Synthesis and Antibacterial Properties of Fluorapatite and FAp-ZnO-Chitosan Composite as Dental Implant Materials

Charlena[1*], Alif Aryan Khofiyatuzziyadah[1], Akhiruddin[2], Purwantiningsih[1]

[1]*Department of Chemistry, Faculty of Science, IPB University, Bogor, West Java, 16680, Indonesia*
[2]*Department of Physics, Faculty of Science, IPB University, Bogor, West Java, 16680, Indonesia*
***Corresponding author**: charlena@apps.ipb.ac.id*

Abstract
Regenerative biomaterials research has continued to grow in recent decades, one of which is dental implants. The material that can be used is fluorapatite (FAp), as it is a significant element of human bones and teeth. FAp has better chemical and thermal stability than other apatite materials. However, FAp has low antibacterial properties, so it needs to be composited with other antibacterial materials, such as zinc oxide (ZnO) and chitosan. In addition, chitosan was also added to stabilize FAp and ZnO in an effort to increase antibacterial and in vitro bioactivity in apatite formation. Therefore, this research intends to synthesize and assess the antibacterial properties and in vitro bioactivity of FAp-ZnO-chitosan to increase its potential as a dental implant manufacturing material. FAp and ZnO were synthesized and then composited with chitosan into FAp-ZnO-chitosan by a simple mixing method. The FAp-ZnO-chitosan composite was successfully synthesized by looking at X-ray diffraction (XRD), Fourier Transform Infra-Red (FTIR), and Scanning Electron Microscope-Energy Dispersive X-ray (SEM-EDX) characterization results. The in vitro bioactivity of the composite showed new surface growth during immersion with simulated body fluid (SBF) solution, indicating potential attachment of the implant material to the tissue. The antibacterial properties of FAp-ZnO-chitosan also showed an increased zone of inhibition compared to the single material. This indicates that the FAp-ZnO-chitosan composite material has the potential to be used as a dental implant material.

Keywords
Antibacterial, Composite FAp-ZnO-Chitosan, Dental Implant, Fluorapatite

Received: 28 November 2024, Accepted: 24 February 2025
https://doi.org/10.26554/sti.2025.10.2.562-573

1. INTRODUCTION

Biomaterials are increasingly important in successfully developing biomedical devices and health tissue engineering. Biomaterials have the potential to replace broken tissues and restore or rebuild normal body functions (Chen and Liu, 2016). Biomaterials for medical applications include bone implants, heart rings, and dental implants. Biomaterials must have bioactivity, biocompatibility, biodegradability, intrinsic bio-signals, low immune response, and antibacterial properties to be safer when applied to the body (Prakasam et al., 2017; Geevarghese et al., 2022).

One application of biomaterials is implants. Implants are usually made of metal or alloys. The use of metals that are easily corroded is a challenge in the medical field. One material that can be used as an implant is apatite material, such as hydroxyapatite (HAp) and fluorapatite (FAp) (Seyedmajidi and Seyedmajidi, 2022). This is because they are the main components of human teeth. FAp has high stability, good hardness, and better thermal properties when compared to HAp due to its fluorine content (Alhilou et al., 2016). Therefore, FAp has more potential to be used for dental implants as it is resistant to acidic environments. In addition, FAp can form when flour at low concentrations in acidic environments interacts with HAp (Zhao et al., 2017). FAp can also release fluoride ions that have osteoconductive and antibacterial properties (Alhilou et al., 2016).

The synthesis of FAp based on gold snail shell waste has been carried out in previous studies using the solid phase reaction method and produced characteristics that are more in line with FAp materials (Khofiyatuzziyadah et al., 2024). Gold snail shells have not been widely used as precursors in the manufacture of FAp. In addition, golden snails are often caught and used as an addition to protein-rich animal feed, while the shells become waste that has not been maximally utilized. FAp synthesis results are widely used in the medical and environmental fields as adsorbents in liquid waste (Billah et al., 2020).

However, further development focuses on the potential of FAp as a dental implant material in the medical field.

FAp contains fluorine which can impact the physical and biological properties of implants in the body. Fluorine in FAp can increase the osteoblastic response to accelerate the remineralization process in bone and tooth growth (Seyedmajidi and Seyedmajidi, 2022). This biomaterial also has advantages in terms of lower resorption and the ability to release fluoride ions that have osteoinductive and antibacterial properties, so it has the potential to be used in medical applications (Alhilou et al., 2016). However, the antibacterial properties of fluorapatite are still relatively low, having an inhibition zone of about 0.24 mm for *Escherichia coli* bacteria (Erlangga et al., 2024). This can be overcome by making composites made from antibacterial materials. Antibacterial materials can be found in inorganic materials such as ZnO and organic materials such as chitosan. Compositing these two materials with FAp has never been done. The combination of inorganic and organic materials is expected to create a synergize that enhances the antibacterial properties of FAp.

Antibacterial activity is currently found in many kinds of metals. One of them is metal oxide, such as zinc oxide (ZnO). ZnO can be used as an antibacterial material because it has high antibacterial activity on various antibacterial strains at a relatively low cost (Manzoor et al., 2016). In addition, ZnO does not increase the pH of the environment, so it does not damage bone tissue (Saha et al., 2010). Therefore, the addition of ZnO is expected to be safer to use to enhance the antibacterial properties of FAp. Antibacterial activity is also affected by particle size. NaOH concentration is essential in controlling particle size (Koutu et al., 2016). Therefore, the variation of NaOH concentration in the study is expected to produce a smaller particle size to enhance its antibacterial properties. However, ZnO compounds, especially nano-sized ones, are thermodynamically unstable in aqueous solutions, so it is necessary to add stabilizers such as chitosan (Yusof et al., 2019).

Besides having antibacterial properties, chitosan is used because it has high osteoinductivity, osteointegration, and biodegr adability characteristics, so it functions as a biomaterial with good bioactive properties and can promote osteoblast growth (Alhilou et al., 2016). The enzymatically breakable nature of chitosan allows it to be broken down in the body, and its degradation products can be naturally metabolized, making chitosan relatively safe for use in biomedical applications (Azaman et al., 2022). Therefore, this research intends to synthesize and assess the antibacterial properties and in vitro bioactivity of FAp-ZnO-chitosan to increase its potential as a dental implant manufacturing material.

2. EXPERIMENTAL SECTION

2.1 Materials

The materials used were $Ca(OH)_2$ (synthesized from golden snail shells), $(NH_4)_2HPO_4$ (Merck), NH_4F (Merck), chitosan (PhyEdumedia), $ZnSO_4.7H_2O$ (Merck), PVP K30 (polyvinyl pyrrolidone) (ALOIN), distilled water, *Streptococcus mutans* bacterial culture, *Escherichia coli* bacterial culture, 2% (v/v) acetic acid and universal pH indicator. The tools used included watch glass, mortar, burette, goblet glass, glass stirrer, magnetic stirrer, funnel, erlenmeyer, drop pipette, Mohr pipette, porcelain crucible, Sanyo MOV-212 oven, Naberthem furnace, Hermle Labnet Z206A centrifuge, Memmert incubator, Origin software, ImageJ software, X'Pert HighScore Plus software, HACH 2100P turbidimeter, FTIR HITACHI 270-50, XRD Rigaku MiniFlex, PSA (Particle Size Analyzer) Horiba Scientific SZ 100z, and SEM-EDX type JSM 6063 LA JEOL.

2.2 Methods

2.2.1 Synthesis of FAp

FAp synthesis refers to Webler et al. (2014). The synthesized $Ca(OH)_2$ compound based on a golden snail shell as a calcium source, $(NH_4)_2HPO_4$ as a phosphate source, and NH_4F as a fluorine source in the ratio of 5:3:1 was mixed and homogenized by grinding for 3 hours. The sample was then calcined at 1000°C for 3 hours to obtain a compact FAp powder.

2.2.2 Synthesis of ZnO

ZnO synthesis followed by Khefanny et al. (2024). $ZnSO_4.7H_2O$ 0.2 M solution with the addition of PVP (polyvinyl pyrrolidone) 15% solution as a stabilizer was subjected to constant stirring at 50°C for 20 min using a magnetic stirrer. NaOH solution of 0.2, 0.4, and 0.8 M was added to the $ZnSO_4.7H_2O$ 0.2 M/PVP mixture drop by drop while stirring at 50°C for 2 hours. The precipitate formed was washed with distilled water until the pH was neutral. Separation was done by centrifuge at 5000 rpm for 20 minutes. The precipitate was dried at 105°C for 3 hours to constant weight. The precipitate was then calcined at 800°C. The ZnO powder was then characterized by XRD, turbidimeter, PSA, and FTIR.

2.2.3 Synthesis of FAp-ZnO-Chitosan Composite

Commercial chitosan was previously characterized by XRD and FTIR. Material compositing refers to Bhowmick et al. (2018). Composite synthesis was carried out by mixing FAp, ZnO, and chitosan in a ratio of 5: 2: 3. FAp was mixed with ZnO in distilled water. The mixture was stirred using a magnetic stirrer for 20 minutes at 500 rpm. Next, chitosan was slowly added to the mixture while stirring. Stirring was continued for 2 hours at 500 rpm at 50°C until homogeneous. The composite formed will be a suspension and then dried in an oven at 60°C for 3 hours until constant weight. The dried composite was ground into powder for further characterization.

2.2.4 Characterization of FAp-ZnO-Chitosan

The composite samples were characterized using a Shimadzu XRD 7000 X-Ray Diffractometer. Diffraction angles were taken at angles 2θ = 10°-80°. The initial angle was 10°, and the final angle was 80°; the reading speed was set at 0.60°/second with a wavelength of 1.5406 Å. The analysis results were further verified by comparing them with the International Center for Diffraction Data (ICDD) database.

Characterization with FTIR (Fourier Transform Infra-red) was also carried out. Samples of 1-2 mg were added with 100-200 mg of KBr. The ratio of the KBr sample is 1:100 to the sample. The sample was ground until smooth and formed into pellets using a compacting tool. The pellets were then inserted into the HITACHI 270-50 FTIR sample holder with a wave number range of 400 to 4000 cm^{-1} for sailing.

The samples were then characterized using SEM-EDX (Scanning Electron Microscope with Energy Dispersive X-Ray Analyzer ThermoFisher Scientific) with the help of gold coating at an accelerating voltage of 12.5 kV and a magnification of 20,000x. The mineral content was then analyzed on the sample. Particle size determination was aided by Origin and ImageJ software.

2.2.5 In Vitro Bioactivity Test

The in vitro bioactivity test refers to Vidhya and Girija (2019). In vitro bioactivity test was conducted by immersing FAp, ZnO, chitosan, and FAp-ZnO-chitosan composite samples in 30 ml SBF (simulated body fluid), then incubated at 37°C for 0, 7, 14, and 21 days. The composition of the SBF solution includes NaCl, KCl, Na_2SO_4, $NaHCO_3$, Na_2HPO_4, $MgCl_2.6H_2O$, $CaCl_2.2H_2O$, and $(CH_2OH)_3CNH_2$ one by one in deionized water and the pH was adjusted to 7.4 using 1 M HCl to match human blood plasma. For 3 weeks, the SBF solution was replaced once in 1 week. Thus, the SBF solution was changed 3 times over 3 weeks. Afterward, the surface of the discs was analyzed using SEM-EDX.

2.2.6 Antibacterial Activity

The antibacterial activity refers to Vidhya and Girija (2019); Salehi et al. (2020); Yousef and Danial (2012). The antibacterial activity of FAp, ZnO, chitosan, and FAp-ZnO-chitosan composite samples was analyzed by disc diffusion method. The microorganisms used were *Streptococcus mutans* (Gram-positive bacteria), commonly found in the mouth, and *Escherichia coli* (Gram-negative bacteria), commonly found in the human body. Bacterial suspensions were cultured using the zigzag technique on agar plates. Test samples were prepared by dissolving FAp, ZnO, FAp-ZnO, and FAp- ZnO-chitosan in 2% acetic acid at 1% concentration, respectively. Discs of 8 mm diameter and 1 mm thick were immersed in the sample solution for ± 30 min. After soaking, the sample discs were placed in a bacterial culture dish by pressing to stick to the dish's surface. Next, the agar plates were incubated for 24 hours at 37 ± 0.5°C. The zone of inhibition can then be calculated.

3. RESULTS AND DISCUSSION

3.1 Fluorapatite Characteristics

Fluorapatite synthesized by the solid phase reaction method showed a diffractogram corresponding to the FAp crystal phase. This is characterized by the presence of distinctive peaks appearing at 2θ = 31.94°, 32.27°, and 33.13° (Figure 1a) in accordance with ICDD No. 00-015-08776. This confirms that FAp crystals have been formed. These peaks are also in accordance with research Borkowski et al. (2020), which confirmed the presence of a typical FAp peak with the highest intensity at an angle of 2θ = 31.91°. The FAp phase on the diffractogram can also be strengthened by identifying the crystallinity of the synthesized material. The diffractogram results in (Figure 1a) show high crystallinity characterized by sharp peaks.

The synthesized FAp shows high crystallinity, which is 88.81%. This is related to the chemical and thermal stability of FAp. The sharper FAp peak indicates an increase in crystallinity, thus increasing the chemical and thermal stability of FAp (Barandehfard et al., 2016). Tredwin et al. (2013) confirmed the thermal stability of HAp, HA-FAp, and FAp by DTA (differential thermal analysis) that increasing fluoride content allows the structures to crystallize more efficiently and thus have lower crystallization temperatures (Table 1). This is consistent with the fact that increasing fluoride substitution results in a more stable structure than HAp.

Table 1. The Crystallization Temperature of the Fluoride- Substituted Apatite Composition Was Determined Using the DTA (Tredwin et al., 2013)

Composition of apatite	Crystallization temperature mean±SD (°C)
$Ca_{10}(PO_4)_6F_2$	467±0.21
$Ca_{10}(PO_4)_6OH_{0.5}F_{1.5}$	470±0.43
$Ca_{10}(PO_4)_6OH_1F_1$	492±1.22
$Ca_{10}(PO_4)_6OH_{1.5}F_{0.5}$	498±0.23
$Ca_{10}(PO_4)_6OH_2$	499±0.65

The morphology of FAp was shown from SEM, while the Ca/P ratio of FAp was confirmed from EDX results. The morphology of FAp-SS showed a uniform rod-shaped and oval shape with a particle size of about 400 nm. However, an agglomeration process has occurred characterized by the presence of fused particles (Figure 1b). This happens due to plastic collisions between particle surfaces, forming new surfaces. The surface formed further makes the particles fused so that agglomeration occurs and increases the particle size (Fereshteh et al., 2015).

3.2 ZnO Characteristics

ZnO synthesis was carried out by the precipitation method. This method can control synthesis parameters, such as temperature, solution pH, stirring speed, stirring time, precipitant concentration, solvent, and surfactant concentration (Kim et al., 2018). Precipitation is also a method that can control particle size with low temperatures (Chithra et al., 2015). The resulting ZnO particle size was expected to be as small as possible to increase antibacterial activity. Some studies reveal that NaOH concentration plays an important role in determining morphology and particle size (Chand et al., 2015). Concentration variations were carried out to see the effect of NaOH concentration on particle size.

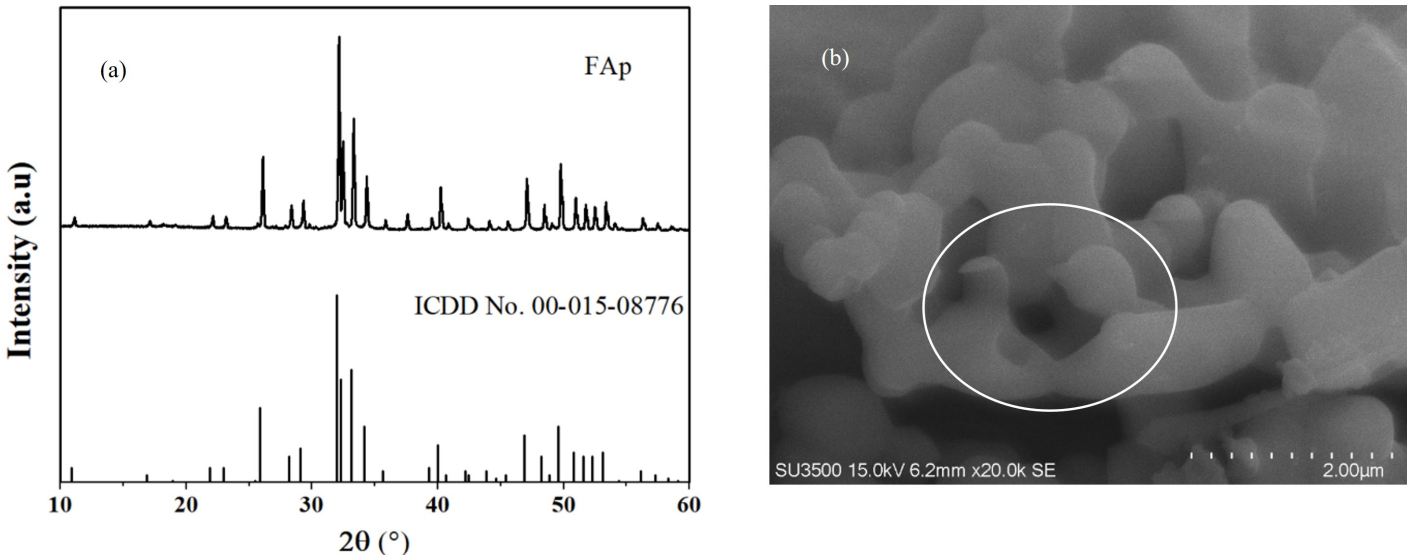

Figure 1. (a) FAp Diffractogram (b) Surface Morphology of FAp Magnification 20000x

The XRD results show that the three variations of NaOH concentration in the synthesis of ZnO produce diffractograms that are in accordance with JCPDS standard No. 36-1451. This is characterized by the presence of 2θ peaks at 31.77°, 34.42°, and 36.25°° (Figure 2). The presence of such peaks indicates confirmed ZnO in accordance with the standard database. This is also confirmed by research Chithra et al. (2015) with the presence of firm diffraction peaks appearing at 2θ angles of 31.80°, 33.40°, and 36.20° indicating the field of wurtzite structure of ZnO crystals in the synthesis. The XRD diffractogram of ZnO was also confirmed by Khefanny et al. (2024), showing a high intensity at angles (2θ) of 31.74° (100), 34.36° (002), and 36.19° (101). The high crystallinity of ZnO for all concentrations indicates that the crystal structure of ZnO is tightly arranged and stable.

The effect of concentration can be seen from the crystallite size, turbidity, and particle size (Table 2). The results of PSA analysis show an increasing trend in size from 200-500 nm as the NaOH concentration increases. This is in line with the crystal size analysis of the ZnO diffractogram and turbidity analysis, i.e., the particle size will increase as the concentration of NaOH added increases. The growth of ZnO crystal structure is influenced by several factors, especially the rate of chemical reaction and the concentration of Zn^{2+} and OH^- ions. The addition of NaOH to the dehydrated zinc sulfate solution triggers the precipitation of $Zn(OH)_2$, which then dissociates into Zn^{2+} and OH^- ions. If the concentration of these ions exceeds a critical value, the precipitation of ZnO nuclei will begin. OH^- ions play an important role in the nucleation process and the growth of ZnO crystals. In addition, increasing the molar concentration will increase the concentration of OH^- ions in the solution, thereby accelerating the growth rate and resulting in a larger ZnO structure (Chand et al., 2015).

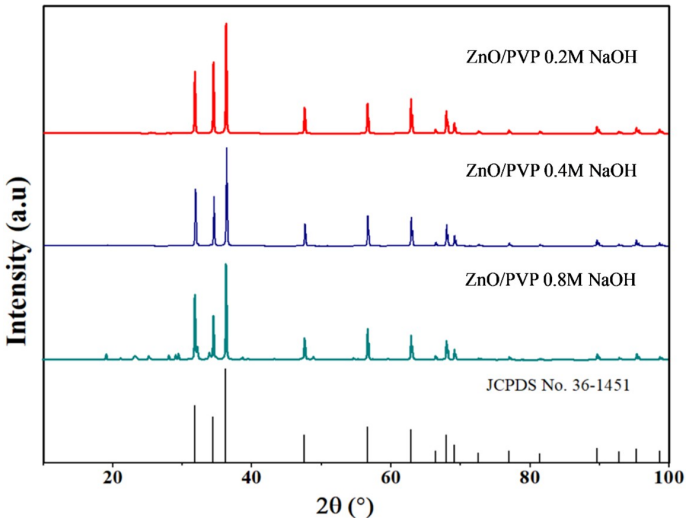

Figure 2. ZnO Diffractogram with Various NaOH Concentrations

3.3 Composite Characteristics

Composite composition is based on the composition of human bones and teeth. Human bones and teeth, especially enamel, are hydrated biological composites, consisting of 70% inorganic material and 30% mixture of organic matrix and water (Basu, 2017). The only organic material used as the main component of the composite is chitosan, so the composition of chitosan is made fixed, namely 30%. Chitosan was chosen because it is a biopolymer that also has the potential to increase the antibacterial properties of FAp (Sutha et al., 2013). The results of the composite synthesis were then characterized by XRD, FTIR, and SEM-EDX, which were compared with the main components.

Table 2. Crystallinity, Crystal Size, Turbidity, and Particle Size ZnO

Sample ZnO	Crystallinity (%)	Size of Crystallite (nm)	Turbidity (NTU)	Particle size (nm)
NaOH 0.2 M	90.00	7.98	303.00	226.43
NaOH 0.4 M	90.01	8.63	368.33	376.14
NaOH 0.8 M	89.47	11.66	611.67	500.56

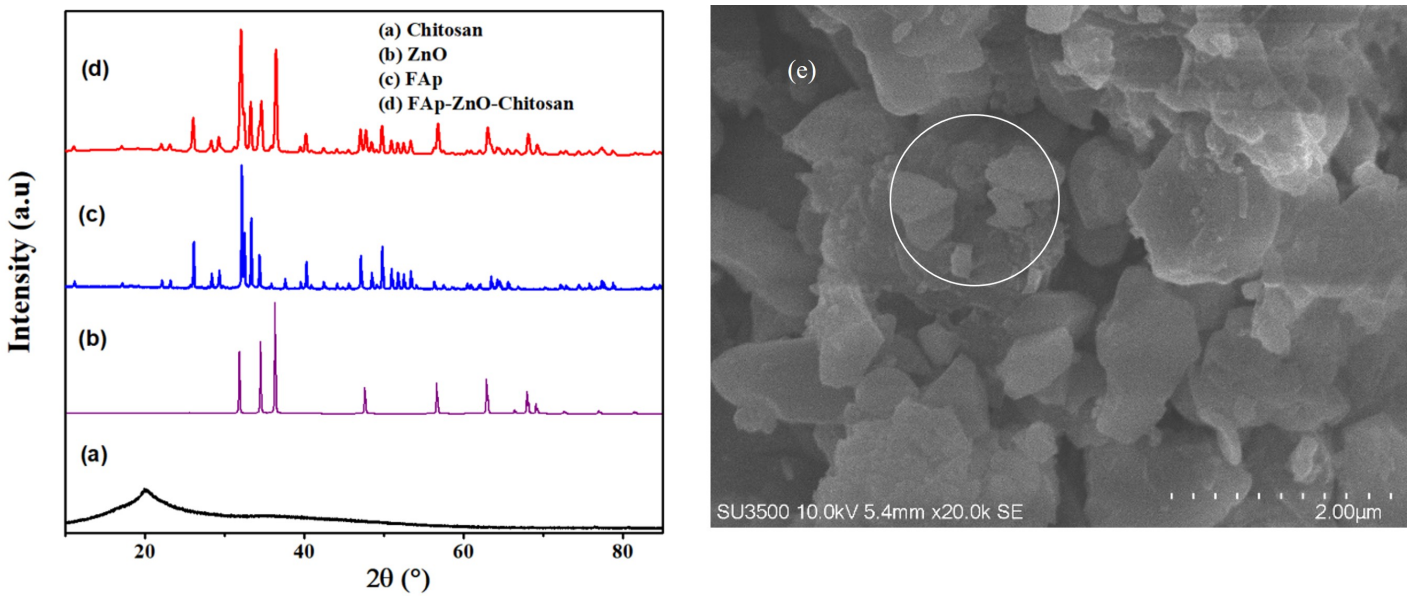

Figure 3. Diffractogram of (a) Chitosan (b) ZnO (c) FAp (d) Composite and (e) Surface Morphology of FAp-ZnO-Chitosan Magnification 20000x

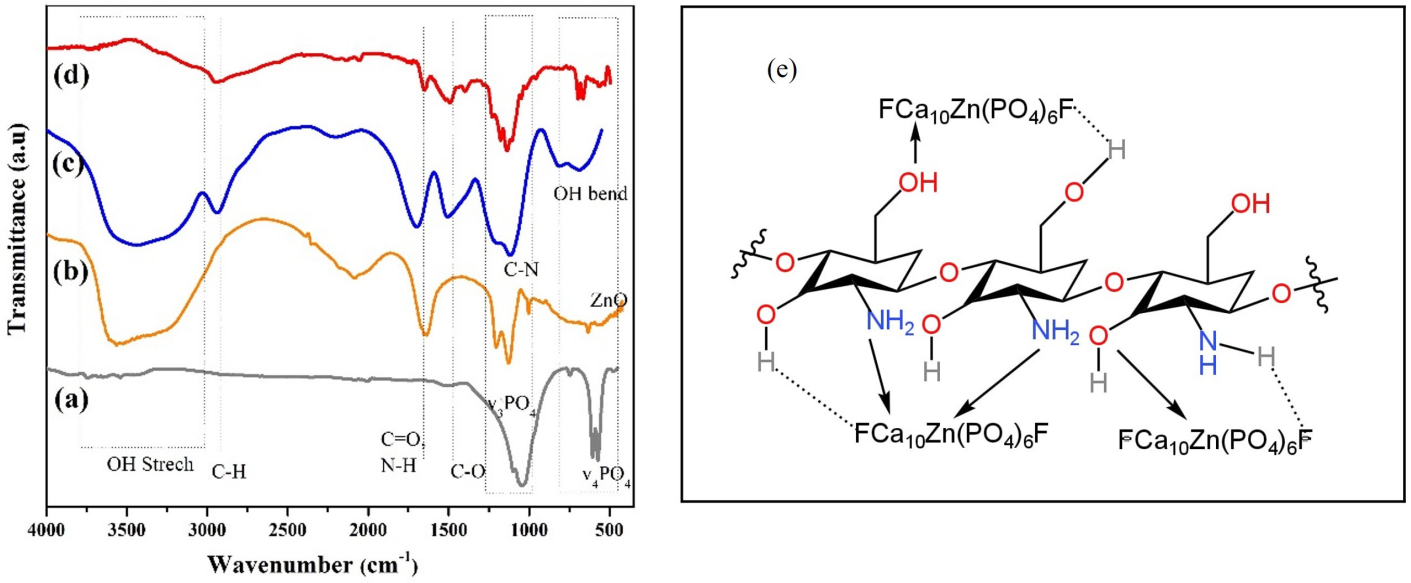

Figure 4. Spectrum IR (a) FAp (b) ZnO (c) Chitosan (d) Composite and (e) Illustration of Interactions That May Occur in FAp-ZnO-Chitosan Composites

The diffractograms of the composites were compared with their constituent materials (Figures 3a-c). The findings of peaks at 2θ angles of 15.18°, 20.30°, 21.30°, and 23.90° (Figure 3a) have shown agreement with the crystalline phase of chitosan in JCPDS No. 039-1894 as the standard for diffractogram analysis. The crystallinity of chitosan from the diffractogram

analysis, which is 31.06%, shows that crystals are more likely to be amorphous. Low crystallinity can be seen from the widened diffractogram and low intensity. The interaction analysis of the composite was further done by comparing the diffractogram of the composite (Figure 3d) with chitosan (Figure 3a), ZnO (Figure 3b), and FAp (Figure 3c).

Table 3. Comparison of Crystallinity and Crystal Size of Composite Constituent Materials

Sample	Crystallinity (%)	Crystal size (nm)
FAp	88.81	7.66
ZnO	90.00	7.98
Chitosan	31.06	5.29
Composite	75.92	6.38

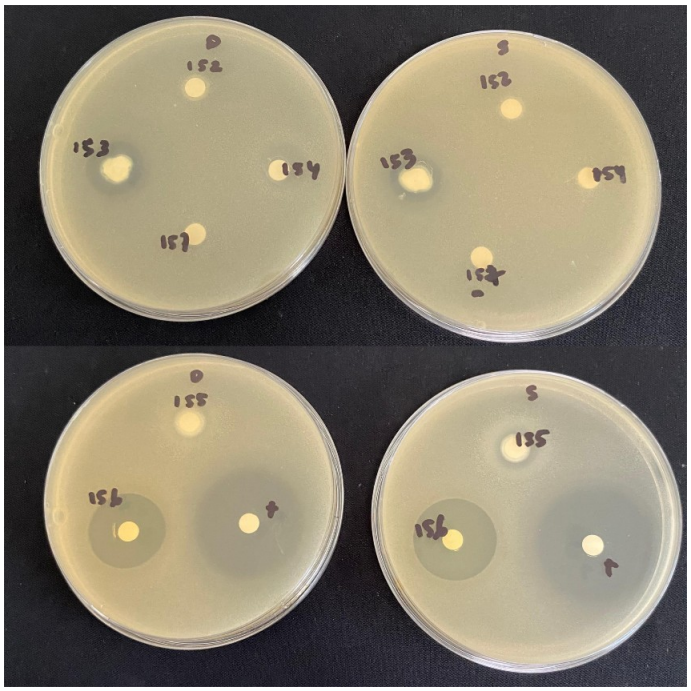

Figure 5. Inhibition Cone of FAp (152), ZnO (153), Chitosan (154), FAp-ZnO (155) and Composites FAp-ZnO-Chitosan (156) Against *S. mutans* Bacteria

The composite diffractograms show the presence of phases of each material. This is indicated by the presence of peaks at 2θ angles of 32.09°, 33.27°, and 34.57° (Figure 3d), which are typical FAp peaks with the highest intensity. The interaction of ZnO with FAp is characterized by a shift in the typical peak of ZnO in the composite, which joins and overlaps with the typical peak of FAp, namely at 2θ 31.77°; 34.42°; 36.25°, to 32.09°; 34.57°; and 36.47° (Figure 3The peaks of 36.47°, 56.83°, 63.06°, 68.16°, and 69.29° are also typical ZnO peaks that appear in the composite material (Figure 3d). In addition, the interaction of the chitosan semicrystalline phase with FAp and ZnO material is characterized by the apparent increase of peaks around 2θ 10-20°. The apparent increase can be caused by the large difference in diffraction peak intensity between FAp and chitosan so that the chitosan peak cannot be seen significantly (Elhendawi et al., 2014).

The surface morphology of the composite at 20000× magnification is observed in Figure 3e. The surface morphology of the composite shows a non-uniform particle shape with a possible particle size of around 468.27 nm. This is due to 3 components with different shapes and sizes colliding with each other and forming agglomerates (Figure 3e). Collisions can occur due to an increase in the kinetic energy of the composite materials due to the heating process during synthesis. Materials with high kinetic energy will close together or intersect to form new bonds and agglomerate. Agglomeration can also occur due to poor interface interaction of the matrix and filler. This can also be influenced by ZnO as a metal material that has a strong attractive force, namely the van der Waals force (Rubel et al., 2019).

The semi-crystalline nature of chitosan cannot show its interaction clearly on the composite diffractogram, but its influence can be seen from the crystallinity and crystal size of the composite (Table 3). This has also been reported by Nikpour et al. (2012), who stated that the crystallinity of apatite material decreased when it was composited with chitosan, which may be due to the interfacial bonding between apatite particles and chitosan matrix. Nikpour et al. (2012) also stated that the composite peaks become slightly broader and weaker than the pure material.

The interaction between FAp, ZnO, and chitosan can be seen from the decrease in crystallinity and crystal size due to the influence of chitosan, which is semicrystalline. Chitosan, which is semicrystalline, can reduce the crystallinity and crystal size of other constituent materials. This is in line with Said et al. (2021) that the decrease in crystallinity of HAp-chitosan composites is explained by an increase in the content of organic phases known for their low crystallinity.

Further characterization was done by looking at the resulting IR spectrum. The spectrum of Figure 4a shows the spectrum of FAp, with a typical peak at the phosphate group, the spectrum of Figure 4b is the spectrum of ZnO with a typical peak at the fingerprint wave number, while Figure 4c is the spectrum of chitosan. The structure of chitosan consists of −OH, N−H, C−H, and C−O detected at 3417 cm^{-1} showing the vibration of −OH overlapping with N-H, 2899 cm^{-1} showing the aliphatic −CH stretching band, and spectra at 1650 cm^{-1} and 1035 cm^{-1} showing the vibration of C−N amine group of chitosan (Fatoni et al., 2023). The IR spectrum of the composite showed the presence of C−H peak at wave number 2904 cm^{-1}, N-H and C=O at wave number 1575 cm^{-1}, C−O at 1412 cm^{-1}, and C−N that accumulates with PO_4^- at wave number 1153-1063 cm^{-1}. The accumulation of peaks and the shift of wave numbers on these peaks indicate the interaction between chitosan and FAp.

The interaction of ZnO with FAp can also be observed at wave numbers 600-400 cm^{-1} which shows the typical absorp-

tion of ZnO. The interaction can be seen from the shift in wave number and the decrease in intensity of the $v4$ PO_4^{3-} group at these wave numbers (Figure 4d). Intannia et al. (2023) also confirmed that the presence of ZnO interacting with apatite material causes the transfer of vibrational energy in apatite molecules, as indicated by a decrease in the intensity of the IR spectrum.

Interactions that may occur on the composite surface are hydrogen bonds and van der Waals forces. Hydrogen bonding can be found when the OH-F group on FAp interacts with the OH group on chitosan. The interaction of FAp and chitosan can also occur between Ca^{2+} ions and F^- ions from FAp with NH_2 or OH groups from chitosan (Venkatesan et al., 2016). The NH_2 group on chitosan also has the potential to form hydrogen bonds with OH-F on FAp (Figure 4e). In addition, the interaction of ZnO with FAp is characterized by a shift and decrease in the intensity of the phosphate group of FAp, especially at wave numbers 559 and 569 cm^{-1}. This phenomenon has been explained Moldovan et al. (2015) which states that the shift and reduction in intensity or removal of peaks in the phosphate group is a result of the interaction of ZnO with PO_4^{3-} from FAp through bidentate coordination with Zn. Zn species in ZnFAp are in tetrahedral geometry, which has an oxidation number of +2 so that it can form a bidentate with the phosphate group of FAp (Moldovan et al., 2015).

The EDX results show the elemental composition of the composite material (Table 4). The basic principle of EDX is to compare the X-ray intensity ratios of the elements contained in the sample at a particular area of the sample. The Ca/P ratio can be analyzed from the EDX results to see the change in the ratio between FAp before composite and after composite. The resulting Ca/P ratio decreased from 1.86 to 1.76 (Table 4). The decrease in Ca/P ratio allows Ca to be substituted with Zn, resulting in a chemically bound ZnFAp. The chemical interaction of Zn in FAp was reported Moldovan et al. (2015) as the interaction of ZnO with PO_4^{3-} of FAp through bidentate coordination with Zn, resulting in ZnFAp material.

The agglomerated particle morphology is made possible by the interaction between materials in the composite (Figure 3e). This is supported by the composite diffractogram, which shows the addition of new peaks in the FAp matrix, namely peaks from ZnO and chitosan fillers, so the composite is confirmed (Figure 3d). Another characterization that supports the interaction between materials to form FAp-ZnO-chitosan composites from the resulting IR spectra (Figures 4a-d). The results of the analysis of the three characteristics show the success of the FAp-ZnO-chitosan composite synthesis.

3.4 In Vitro Bioactivity Properties

The in vitro bioactivity of a composite refers to the ability of the material to facilitate the formation of a strong interfacial bond between the implant and the surrounding living tissue. Vidhya and Girija (2019). Ceramic bioactivity has been defined as the ability to bond with host bone tissue. This includes enhancing apatite formation ability, osteoblast differentiation, and bone

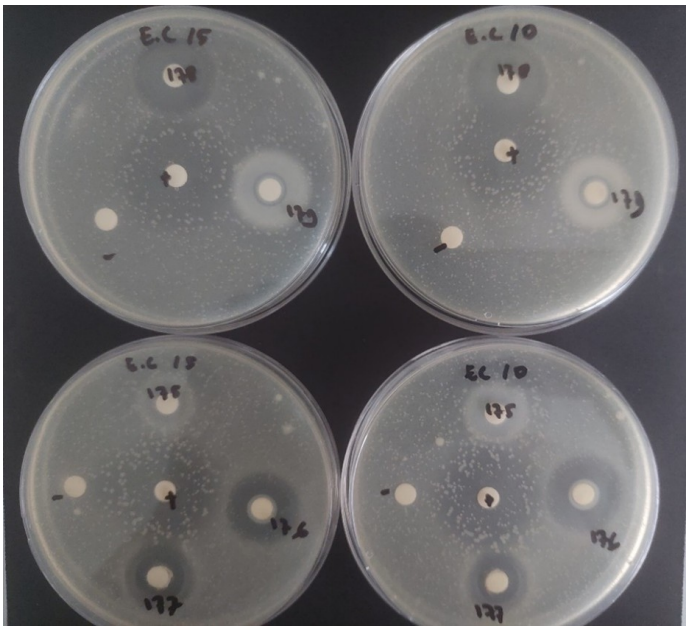

Figure 6. Inhibition Zone of FAp (175), ZnO (176), Chitosan (177), FAp-ZnO (178), and Composites FAp-ZnO-Chitosan (179) Against *E. coli* Bacteria

matrix formation. One method of in vitro bioactivity testing is the SBF method. The SBF method is a helpful way to test the bioactivity of bioceramics in vitro to assess the potential for apatite formation (Wu and Xiao, 2009).

The fabrication of the calcium phosphate (CaP) layer on the scaffold surface during the immersion process in Simulated Body Fluid (SBF) can be observed through Scanning Electron Microscopy (SEM) images, as shown in Figure 7. The surfaces of samples K0, K7, K14, and K21 were immersed in SBF starting from 0, 7, 14, and 21 days. The K0 sample showed a plain surface with many pores, while the more extended the immersion in SBF, the surface of the sample began to form a new surface. The formation of apatite deposits is triggered by the release of large amounts of calcium ions from the matrix during the dissolution process. These calcium ions then interact with phosphate in the SBF to form calcium phosphate, which further results in the formation of nuclei and growth of FAp particles on the sample surface (Vidhya and Girija, 2019).

The in vitro bioactivity of the composite is also shown from the EDX results that the Ca/P ratio decreases with increasing days. This is because the exchange of Ca with Na in SBF indicates the activity of the composite (Table 5). The precipitate formed due to the interaction of ions in the SBF solution forms a new layer. During the immersion process in SBF, apatite layers form and fill the pores of the composite. SBF is a metastable calcium phosphate solution saturated with apatite, thus allowing the formation of apatite layers through a series of chemical reactions, including spontaneous precipitation, nucleation, and growth of calcium phosphate. In this process, FAp particles in the composite scaffold consisting of ZnO and chitosan serve

Table 4. Comparison of Elemental Composition and Ratio of Ca/P FAp With FAp-ZnO-Chitosan Composites

FAp-SS			FAp-ZnO-chitosan composite		
Element	Mass (%)	Ca/P	Element	Mass (%)	Ca/P
Ca	40.45		Ca	33.80	
P	16.82		P	14.86	
F	3.51	1.86	Na	0.69	1.76
C	3.91		O	44.57	
O	35.31		Zn	6.09	

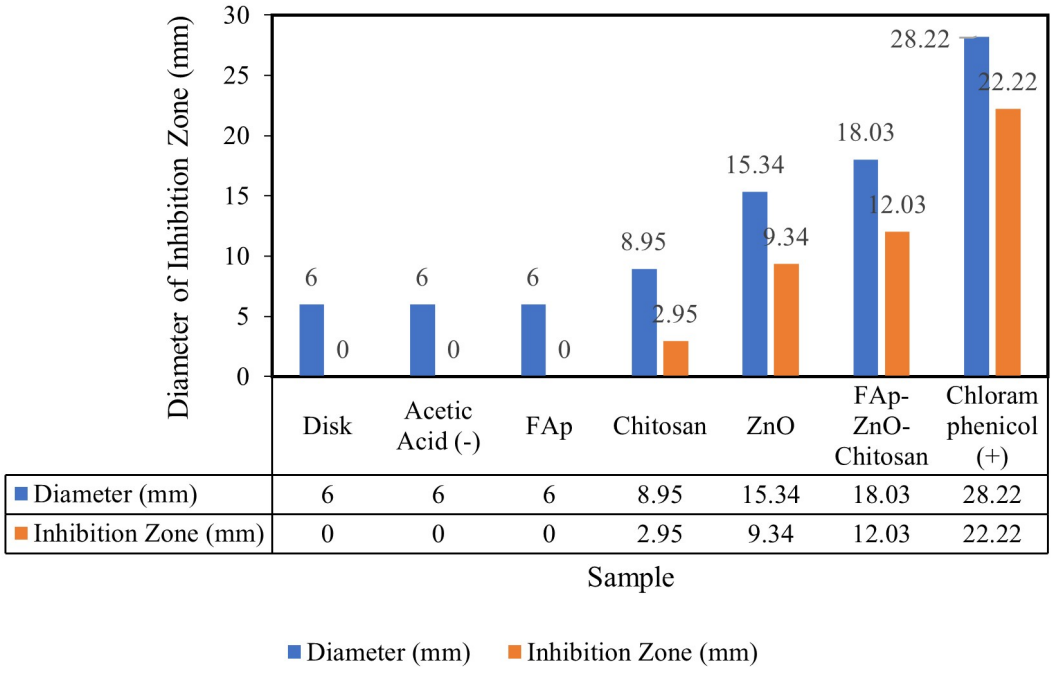

Figure 7. Antibacterial Properties of FAp, ZnO, Chitosan, and Composites Against *S. mutans* Bacteria

as the core for the mineralization process. (Tondnevis et al., 2019).

In addition, the ability of a scaffold to control cell adhesion to its surface is critical in the design of substrates for tissue engineering applications. Cell adhesion affects various aspects of cellular function, such as growth, spreading, migration, proliferation and differentiation. Surface energy and scaffold composition are the main factors that influence cell adhesion. Therefore, the addition of chitosan to the scaffold can facilitate cell adhesion through the pores of the scaffold and increase surface hydrophilicity (Tondnevis et al., 2019).

3.5 Antibacterial Properties

Antibacterials play a role in disrupting the growth and development of bacteria or killing bacteria. Antibacterial testing uses *Streptococcus mutans* and *Escherichia coli* bacteria. *S. mutans* bacteria are Gram-positive bacteria that are commonly found in human teeth, while *E. coli* are Gram-negative bacteria that are commonly found in the human body. Antibacterial activity can be determined using the diameter of the inhibition zone. Bacteria are defined as resistant to the material if they have an inhibition zone diameter ≤9 mm, sensitive with an inhibition zone diameter of 10-11 mm, or very sensitive with an inhibition zone diameter ≥12 mm against the test material (Addo-Mensah and Holland, 2022). In addition, Sanam et al. (2022) stated that antibacterial activity is weak if the diameter of the inhibition zone is ≤5 mm, moderate category 5-10 mm, strong category 10-20 mm, and categorized as very strong if ≥ 20 mm.

The results of antibacterial testing showed that there was no clear zone visible on FAp, both on *S. mutans* bacteria (Figure 5) and on *E. coli* bacteria (Figure 6). The antibacterial properties of FAp may be influenced by the concentration of flour ions in FAp. The fluoride concentration required for the antibacterial effect largely exceeds the concentration required to reduce the solubility of apatite, so to maintain the apatite properties, an appropriate fluorine concentration is required (Kus-Liśkiewicz et al., 2019). This makes it possible that FAp did not show a

Table 5. Comparison of Elemental Composition and Ratio of Ca/P FAp-ZnO-Chitosan Composites in SBF Solution

Element	K0		K7		K14		K21	
	% atom	Ca/P	% atom	Ca/P	% atom	Ca/P	% atom	Ca/P
Ca	13.10	1.95	14.77	1.82	8.20	1.81	12.82	1.71
P	6.71		8.10		4.52		7.47	
F	1.29		1.03		0.69		2.45	
Zn	7.00	1.96	2.55	1.68				
C	30.93		19.00		34.54		28.06	
O	40.98		32.77		33.28		37.85	
Na	-		11.38		6.46		3.62	
Cl	-		10.98		9.75		6.04	

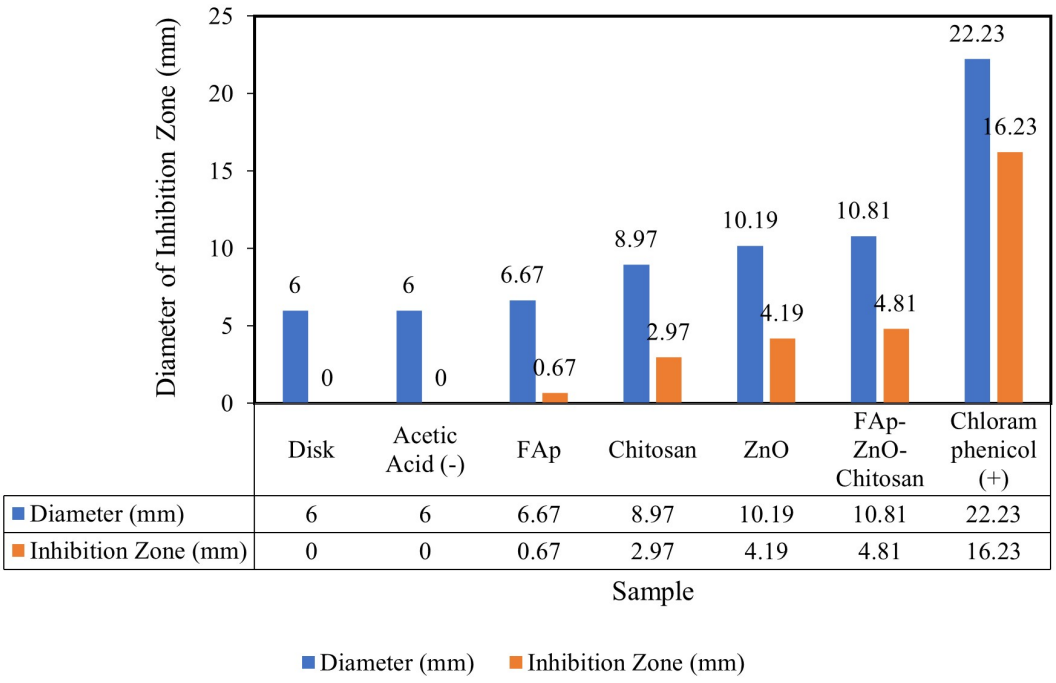

Figure 8. Antibacterial Properties of FAp, ZnO, Chitosan, and Composites Against *E. coli* Bacteria

clear zone in the antibacterial activity test.

The antibacterial properties of chitosan are more effective against Gram-negative bacteria. This can be seen from the clear zone on *E. coli* bacteria (Figure 6), while chitosan did not confirm the clear zone on *S. mutans* bacteria (Figure 5). Electrostatic imbalance is very strong against Gram-negative bacteria, where phosphate-rich lipopolysaccharides are very susceptible to interacting with chitosan (Gritsch, 2019). In addition, the outer membrane of Gram-positive bacteria does not contain many phosphate groups, making chitosan resistant to Gram-positive bacteria. This allows single chitosan not to show a clear zone, such as FAp in the antibacterial activity test on *S. mutans* which is a Gram-positive bacterium.

ZnO material shows a clear zone categorized as medium, which is 6.39 mm (Figure 7). This shows that ZnO has the potential to be composited with FAp to increase the antibacterial properties of FAp. The results showed that FAp composited with ZnO and chitosan produced a synergy effect in increasing the antibacterial activity of FAp, with the inhibition zone reaching 9.08 mm, categorized as moderate and sensitive (Figure 7). In addition, the antibacterial properties of the FAp-ZnO-chitosan composite against *E. coli* bacteria were categorized as weak, with an inhibition zone of 4.81 mm (Figure 8). This shows that the FAp-ZnO-chitosan composite is more effective on Gram-positive bacteria, namely *S. mutans*.

Dental implant materials need to have antibacterial properties against *S. mutans* bacteria because these bacteria can cause dental caries. This is because *S. mutans* can produce large amounts of glucan and acid beyond the buffering capacity of saliva. In addition, this bacterium can also survive in an acidic environment, making it a major pathogen for human teeth (Almoudi et al., 2018). The study showed that FAp-ZnO-chitosan

composites are more effective against *S. mutans* bacteria compared to *E. coli* and thus have more potential to be used as dental implants.

The antibacterial activity of FAp and FAp-ZnO with clear zones has also been carried out by Salehi et al. (2020) against *S. aureus* and *E. coli*. The results showed no inhibition zone for pure FAp powder but the incorporation of ZnO in the structure of FAp powder significantly enhanced its antibacterial activity. In addition, the activity of ZnO-chitosan was also reported by Petkova et al. (2014) that ZnO-chitosan composites produce a synergy effect compared to the single material. The compositing led to a reduction in bacterial growth for *S. aureus* after 60 minutes reaching 98% while ZnO and chitosan alone reduced bacterial growth by 61% and 31%, respectively.

The antibacterial activity of the FAp-ZnO-chitosan composite that reached 9.08 mm was most influenced by ZnO because, in its single material, ZnO produced antibacterial properties with an inhibition zone of 6.39 mm. At the same time, FAp and chitosan showed no observed inhibition zone (Figure 7). ZnO material is the main contributor to improving the antibacterial properties of FAp. The addition of chitosan can also be explained by the interaction between Zn metal ions and chitosan.

The active side of chitosan and metal ions can form complexes according to Lewis acid-base theory. Zn^{2+} ions act as electron acceptors, and chitosan acts as a Lewis base that forms a chelate reaction through a coordinate bond between the N aton of the NH_2 or O group of the OH group on chitosan. The antibacterial activity of the FAp-ZnO-chitosan composite is due to the chelate reaction formed from chitosan and metal ions interact with the outer surface of bacterial cells and disrupt the cytoplasmic membrane. The chitosan and Zn^{2+} ions cross-linked, thus increasing the Zn^{2+} content in Gram-positive and Gram-negative bacteria. This is because the outer layer of the bacterial cell contains pores that transport charges through the membrane, so the interaction of the bacterial cell with the substrate depends on its surface charge (Singh and Dubey, 2018). This is what can inhibit the activity of pathogenic bacteria.

4. CONCLUSIONS

FAp-ZnO-chitosan composite was successfully synthesized and confirmed through XRD, FTIR, and SEM-EDX characterization. The three characteristics have supported each other in successfully synthesizing the FAp-ZnO-chitosan composite. The success of the synthesis was indicated by the interactions between materials, such as the presence of hydrogen bonds and coordination bonds that occur. The in vitro bioactivity of FAp-ZnO-chitosan composite showed the formation of new surfaces during immersion in SBF solution. The antibacterial activity of the composite is also better than each of its constituent materials, namely FAp, ZnO, and chitosan, characterized by an increase in the clear zone of the antibacterial test. In addition, the antibacterial activity of the composite is higher on *S. mutans* bacteria, which are Gram-positive bacteria often found in the mouth, than on *E. coli* bacteria, which are Gram-negative bacteria often found in the human body. The analysis of the composite showed that the material has more potential to be used as a dental implant.

5. ACKNOWLEDGEMENT

This time, the author would like to express gratitude to the Ministry of Education, Culture, Research and Technology has provided funding for this research through the Penelitian Pascasarjana-Proposal Tesis Magister (PPS-PTM) scheme in 2024 Number: 027/ES/PG.02.00.PL/2024 dated June 11, 2024. The author also expresses gratitude to the Laboratory of Inorganic Chemistry of IPB University for enabling the author to do research at the lab to complete this final project properly.

REFERENCES

Addo-Mensah, A. and D. P. Holland (2022). Evaluation of the Antimicrobial Activity of Vangueria Volkensii Bark, Fruit, Leaf, and Stem Extracts. *J. Med. Plants*, **10**(2); 208–214

Alhilou, A., T. Do, L. Mizban, B. H. Clarkson, D. J. Wood, and M. G. Katsikogianni (2016). Physicochemical and Antibacterial Characterization of a Novel Fluorapatite Coating. *ACS Omega*, **1**(2); 264–276

Almoudi, M. M., A. S. Hussein, M. I. A. Hassan, and N. M. Zain (2018). A Systematic Review on Antibacterial Activity of Zinc Against Streptococcus Mutans. *The Saudi Dental Journal*, **30**(4); 283–291

Azaman, F. A., K. Zhou, M. D. M. Blanes-Martínez, M. Brennan Fournet, and D. M. Devine (2022). Bioresorbable Chitosan-Based Bone Regeneration Scaffold Using Various Bioceramics and the Alteration of Photoinitiator Concentration in an Extended UV Photocrosslinking Reaction. *Gels*, **8**(11); 696

Barandehfard, F., M. K. Rad, A. Hosseinnia, K. Khoshroo, M. Tahriri, H. E. Jazayeri, and L. Tayebi (2016). The Addition of Synthesized Hydroxyapatite and Fluorapatite Nanoparticles to a Glass-Ionomer Cement for Dental Restoration and Its Effects on Mechanical Properties. *Ceramics International*, **42**(15); 17866–17875

Basu, B. (2017). Natural Bone and Tooth: Structure and Properties; 45–85

Bhowmick, A., S. L. Banerjee, N. Pramanik, P. Jana, T. Mitra, A. Gnanamani, M. Das, and P. P. Kundu (2018). Organically Modified Clay Supported Chitosan/Hydroxyapatite-Zinc Oxide Nanocomposites with Enhanced Mechanical and Biological Properties for the Application in Bone Tissue Engineering. *International Journal of Biological and Macromolecules*, **106**; 11–9

Billah, R. E. K., Y. Abdellaoui, Z. Anfar, G. Giácoman-Vallejos, M. Agunaou, and A. Soufiane (2020). Synthesis and Characterization of Chitosan/Fluorapatite Composites for the Removal of Cr (VI) from Aqueous Solutions and Optimized Parameters. *Water, Air, and Soil Pollution*, **231**; 1–14

Borkowski, L., A. Przekora, A. Belcarz, K. Palka, G. Jozefaciuk, T. Lübek, and G. Ginalska (2020). Fluorapatite Ceramics

for Bone Tissue Regeneration: Synthesis, Characterization, and Assessment of Biomedical Potential. *Materials Science and Engineering: C*, **116**; 1–10

Chand, P., A. Gaur, A. Kumar, and U. K. Gaur (2015). Effect of NaOH Molar Concentration on Optical and Ferroelectric Properties of ZnO Nanostructures. *Applied Surface Science*, **356**; 438–446

Chen, F. M. and X. Liu (2016). Advancing Biomaterials of Human Origin for Tissue Engineering. *Progress in Polymer Science*, **53**; 86–168

Chithra, M., M. Sathya, and K. Pushpanathan (2015). Effect of pH on Crystal Size and Photoluminescence Property of ZnO Nanoparticles Prepared by Chemical Precipitation Method. *Acta Metallurgica Sinica (English Letters)*, **28**(3); 394–404

Elhendawi, H., R. M. Felfel, B. M. Abd El-Hady, and F. M. Reicha (2014). Effect of Synthesis Temperature on the Crystallization and Growth of in situ Prepared Nanohydroxyapatite in Chitosan Matrix. *ISRN Biomaterials*, **2014**; 1–8

Erlangga, M., C. Charlena, and I. H. Suparto (2024). Synthesis and Characterization of Fluorapatite-Copper (II) Oxide with Sol-Gel Method as an Antibacterial Biomaterial. *Jurnal Kimia Sains dan Aplikasi*, **27**(4); 174–181

Fatoni, A., V. F. Hidayah, S. Suyata, H. Diastuti, and M. D. Anggraeni (2023). Chitosan–Fe3O4 Nanoparticles Cryogel for Glucose Biosensor Development. *Science and Technology Indonesia*, **8**(1); 52–58

Fereshteh, Z., M. Fathi, and R. Mozaffarinia (2015). Synthesis and Characterization of Fluorapatite Nanoparticles via a Mechanochemical Method. *Journal of Cluster Science*, **26**(4); 1041–1053

Geevarghese, R., S. S. Sąjjadi, A. Hudecki, S. Sąjjadi, N. R. Jalal, T. Madrakian, and M. J. Łos (2022). Biodegradable and Non-biodegradable Biomaterials and Their Effect on Cell Differentiation. *International Journal of Molecular Sciences*, **23**(24); 16185

Gritsch, L. (2019). *An Investigation on Antibiotic-Free Antibacterial Materials Combining Bioresorbable Polyesters, Chitosan and Therapeutic Ions*. Ph.D. thesis, Friedrich-Alexander-Universität Erlangen-Nürnberg (FAU)

Intannia, W., C. Charlena, and I. H. Suparto (2023). Hydroxyapatite-ZnO Biomimetic Toothpaste Formulation from Rice Snail Shell Waste. *Science and Technology Indonesia*, **8**(3); 486–493

Khefanny, Y. C., C. Charlena, and S. Sugiarti (2024). Synthesis and Characterization of ZnO/Cellulose Acetate Composite and Its Activity as Antibacterial Agent. *Science and Technology Indonesia*, **9**(2); 215–223

Khofiyatuzziyadah, A. A., C. Charlena, and A. Maddu (2024). Synthesis and Characterization of Golden Snail Shell-based Fluorapatite via Precipitation and Solid-State Reaction Methods. *Materials International*, **6**(4); 1–12

Kim, G., J. Kim, and H. Youn (2018). Effect of Temperature, pH, and Reaction Duration on Microbially Induced Calcite Precipitation. *Applied Sciences*, **8**(8); 1277

Koutu, V., L. Shastri, and M. M. Malik (2016). Effect of NaOH Concentration on Optical Properties of Zinc Oxide Nanoparticles. *Materials Science-Poland*, **34**(4); 819–827

Kus-Liśkiewicz, M., J. Rzeszutko, Y. Bobitski, A. Barylyak, G. Nechyporenko, V. Zinchenko, and J. Zebrowski (2019). Alternative Approach for Fighting Bacteria and Fungi: Use of Modified Fluorapatite. *Journal of Biomedical Nanotechnology*, **15**(4); 848–855

Manzoor, U., S. Siddique, R. Ahmed, Z. Noreen, H. Bokhari, and I. Ahmad (2016). Antibacterial, Structural and Optical Characterization of Mechano-Chemically Prepared ZnO Nanoparticles. *PLoS One*, **11**(5); 1–12

Moldovan, M., D. Prodan, V. Popescu, C. Prejmerean, C. Saroși, M. Saplonţai, and E. Vasile (2015). Structural and Morphological Properties of HA-ZnO Powders Prepared for Biomaterials. *Open Chemistry*, **13**(1); 725–733

Nikpour, M. R., S. M. Rabiee, and M. Jahanshahi (2012). Synthesis and Characterization of Hydroxyapatite/Chitosan Nanocomposite Materials for Medical Engineering Applications. *Composites Part B: Engineering*, **43**(4); 1881–1886

Petkova, P., A. Francesko, M. M. Fernandes, E. Mendoza, I. Perelshtein, A. Gedanken, and T. Tzanov (2014). Sonochemical Coating of Textiles with Hybrid ZnO/Chitosan Antimicrobial Nanoparticles. *ACS Applied Materials and Interfaces*, **6**(2); 1164–1172

Prakasam, M., J. Locs, K. Salma-Ancane, D. Loca, A. Largeteau, and L. Berzina-Cimdina (2017). Biodegradable Materials and Metallic Implants—a Review. *Journal of Functional Biomaterials*, **8**(4); 44

Rubel, R. I., M. H. Ali, M. A. Jafor, and M. M. Alam (2019). Carbon Nanotubes Agglomeration in Reinforced Composites: A Review. *AIMS Materials Science*, **6**(5); 756–780

Saha, N., K. Keskinbora, E. Suvaci, and B. Basu (2010). Sintering, Microstructure, Mechanical, and Antimicrobial Properties of HAp-ZnO Biocomposites. *Journal of Biomedical Materials Research Part B: Applied Biomaterials*, **95**(2); 430–440

Said, H. A., H. Noukrati, H. Ben Youcef, A. Bayoussef, H. Oudadesse, and A. Barroug (2021). Mechanical Behavior of Hydroxyapatite-Chitosan Composite: Effect of Processing Parameters. *Minerals*, **11**(2); 213

Salehi, S., M. Kharaziha, M. Salehi, and V. Saidi (2020). In situ Synthesis of Fluorapatite-ZnO Nanocomposite Powder via Mechanical Alloying for Biomedical Applications. *International Journal of Applied Ceramic Technology*, **17**(4); 1998–2007

Sanam, M. U., A. I. Detha, and N. K. Rohi (2022). Detection of Antibacterial Activity of Lactic Acid Bacteria, Isolated from Sumba Mare's Milk, Against *Bacillus cereus*, *Staphylococcus aureus*, and *Escherichia coli*. *Journal of Advanced Veterinary and Animal Research*, **9**(1); 53

Seyedmajidi, S. and M. Seyedmajidi (2022). Fluorapatite: A Review of Synthesis, Properties and Medical Applications vs Hydroxyapatite. *Iranian Journal of Materials Science and Engineering*, **19**(2); 1–20

Singh, A. and A. K. Dubey (2018). Various Biomaterials and

Techniques for Improving Antibacterial Response. *ACS Applied Bio Materials*, **1**(1); 3–20

Sutha, S., K. Kavitha, G. Karunakaran, and V. Rajendran (2013). In-Vitro Bioactivity, Biocorrosion and Antibacterial Activity of Silicon Integrated Hydroxyapatite/Chitosan Composite Coating on 316 L Stainless Steel Implants. *Materials Science and Engineering: C*, **33**(7); 4046–4054

Tondnevis, F., M. A. Ketabi, R. Fekrazad, A. Sadeghi, and M. M. Abolhasani (2019). Using Chitosan Besides Nano Hydroxyapatite and Fluorohydroxyapatite Boost Dental Pulp Stem Cell Proliferation. *Journal of Biomimetics, Biomaterials and Biomedical Engineering*, **42**; 39–50

Tredwin, C. J., A. M. Young, G. Georgiou, S. H. Shin, H. W. Kim, and J. C. Knowles (2013). Hydroxyapatite, Fluor-Hydroxyapatite and Fluorapatite Produced via The Sol–Gel Method: Optimisation, Characterisation, and Rheology. *Dental Materials*, **29**(2); 166–173

Venkatesan, J., R. Jayakumar, S. Anil, and S. K. Kim (2016). *Nanocomposites for Musculoskeletal Tissue Regeneration*. Woodhead Publishing, Cambridge, UK

Vidhya, G. and E. K. Girija (2019). Comparative Study of Hydroxyapatite Prepared from Eggshells and Synthetic Precursors by Microwave Irradiation Method for Medical Applications. *Materials Today: Proceedings*, **15**; 344–352

Webler, G. D., M. J. M. Zapata, L. C. Agra, E. Barreto, A. O. S. Silva, J. M. Hickmann, and E. J. S. Fonseca (2014). Characterization and Evaluation of Cytotoxicity of Biphasic Calcium Phosphate Synthesized by a Solid-State Reaction Route. *Current Applied Physics*, **14**(6); 876–880

Wu, C. and Y. Xiao (2009). Evaluation of The in Vitro Bioactivity of Bioceramics. *Bone and Tissue Regeneration Insights*, **2**(1); 25–29

Yousef, J. M. and E. N. Danial (2012). In Vitro Antibacterial Activity and Minimum Inhibitory Concentration of Zinc Oxide and Nano-Particle Zinc Oxide Against Pathogenic Strains. *J Health Sci*, **2**(4); 38–42

Yusof, N. A. A., N. M. Zain, and N. Pauzi (2019). Synthesis of ZnO Nanoparticles with Chitosan as Stabilizing Agent and Their Antibacterial Properties Against Gram-Positive and Gram-Negative Bacteria. *International Journal of Biological Macromolecules*, **124**; 1132–1136

Zhao, I. S., M. L. Mei, Q. L. Li, E. C. M. Lo, and C. H. Chu (2017). Arresting Simulated Dentine Caries with Adjunctive Application of Silver Nitrate Solution and Sodium Fluoride Varnish: An In Vitro Study. *International Dental Journal*, **67**(4); 206–214

